Tutor

Dr. Francesc Viñes Solana
Departament de Ciència de Materials i Química Física

Treball Final de Grau

CO Stability on *hcp* Metals

Estabilitat de CO en metalls *hcp*

David Vázquez Parga

July 2020

Lo importante en la ciencia no es tanto obtener nuevos datos, sino descubrir nuevas formas de pensar sobre ellos.

William Lawrence Bragg

Voldria agrair a totes aquelles persones que m'han ajudat a arribar aquí, a la meva família, a Carol per escoltar les meves bogeries tot aquest temps, a Andrea Stefania animar-me a treure lo millor de mi, a Andrea, Martí, Mike, Silvia, Artur, Raquel, Dani, Fileto, Eva i Paola per haver estat sempre allà quan ho necessitava. També vull agrair al meu tutor, Francesc Viñes el haver-me donat la oportunitat per aprendre tant durant aquest treball.

REPORT

CONTENTS

1. SUMMARY

Carbon monoxide (CO) has been used as a probe molecule to study, typically, the chemical activity of Transition Metals (*TMs*) surfaces, but its study has been normally focused on those TMs with a face-centered cubic (*fcc*) crystalline structure, which are close in the Periodic Table, and so, perhaps, does not allow capturing reliable trends along the *d* series. Here we analyze such trends on hexagonal closed-pack (*hcp*) TMs by means of theoretical simulations, here relying on the accuracy of Density Functional Theory (*DFT*) using the Perdew-Burke-Ernzerhof (*PBE*) exchange-correlation functional using suitable slab models.

The detailed analysis of the obtained results allows disentangling different trends, alongside with particular surface reconstructions and CO adsorption modes no previously reported in the literature. Those TMs with low number of valence *d* electrons adsorb the CO stronger, specially connecting its two atoms. While the number of *d* electrons increase, the CO changes to be adsorbed only through the C atom, up to being no adsorbed. This trend goes along quantitatively with the *d*-band centre descriptor model, but qualitatively with the surface energy or the C-metal distance ones. The bonding analysis reveals a donation/back-donation mechanism, which eventually weakens the CO bond order, and so, makes its bonds longer. This has a direct effect, *e.g.* on the simulated infrared (IR) spectra, implying lower frequencies for the CO bond stretching vibration, which can become invisible when the CO molecule adsorbs parallel to surface due to the surface dipole selection rule. Furthermore, the results on the CO dissociation energy reveals that such a metal surface catalysed process is thermodynamically favourable for earlier TMs, but grows endothermic when going along the *d* series.

Keywords: Density Functional Calculations, *hcp* Transition Metals, CO, Adsorption, Dissociation, Infrared Spectroscopy

2. RESUM

La molècula de monòxid de carboni (CO) s'ha utilitzat com a molècula proba per estudiar, típicament, l'activitat química de les superfícies de metalls de transició (*Transition Metals - TMs*), però el seu estudi està normalment enfocat en aquells TMs amb estructura cristallina cubica centrada en les cares (*face centered cubic - fcc*), que son propers en la taula periòdica, i per tant, existeix la possibilitat que no representin una tendència aplicable a la sèrie *d*. Aquí s'analitzaran aquestes tendències en els TMs d'estructura hexagonal compacte (*hexagonal close-packed - hcp*) utilitzant simulacions teòriques, aprofitant la exactitud del teoria del funcional de la densitat (*Density Functional Theory - DFT*) emprant el funcional de correlació i intercanvi Perdew-Burke-Ernzerhof (*PBE*) i utilitzant models de llesca.

L'anàlisi detallat dels resultats obtinguts permet discernir diverses tendències, a més de reconstruccions a particulars superfícies i modes d'adsorció del CO no reportats prèviament a la literatura. Aquells TMs amb baix nombre d'electrons d de valència adsorbeixen el CO més fortament, especialment connectant-se per ambdós àtoms. Al augmentar aquest nombre d'electrons *d*, el CO s'adsorbeix només pel C, i posteriorment per no és adsorbit. Aquesta tendència també es segueix quantitativament amb el descriptor del centre de la banda *d*, però només qualitativament amb l'energia de la superfície o la distancia C-metall. L'anàlisi de l'enllaç revela que el procés de donació/retro-donació afebleix l'enllaç CO i l'allarga. Aquest fet té afecte directe en, per exemple, l'espectre infraroig (*IR*) simulat, implicant freqüències de vibració més baixes per el allargament (*streching*) del enllaç CO, que poden tornar-se invisibles si la molècula s'adsorbeix paral·lelament degut a la regla de selecció del dipol de superfície. Finalment, els resultats de l'energia de dissociació del CO revelen que en aquestes superfícies aquest procés catalític és termodinàmicament favorable per els primer TMs, però més endotèrmic a mesura que s'avança en la sèrie *d*.

Paraules clau: Càlculs del funcional de la densitat, Metalls de transició *hcp*, CO, Adsorció, Dissociació, Espectroscòpia d'infraroig

3. INTRODUCTION

The carbon monoxide (CO) molecule has been extensively used as a probe molecule in Surface Science, as the detail of its adsorption on many materials surfaces —mostly metal surfaces— allows indirectly disentangling atomistic information of them, this is, helping to determine their chemical activity through the strength of the interaction between it and the adsorbed CO, as can be achieved, *e.g.*, by analysing the CO bond stretching vibration frequency by infrared (IR) means. To this end, it becomes of utmost importance to gain atomistic knowledge of this process and the factors that may bias it. This way it would be possible to know not only the trends this process follows with respect certain physicochemical descriptors —variable properties that govern the chemical activity, here expressed through the CO adsorption— but also to be in position of predicting the adsorption process in other more complex, less accessible cases.

Such knowledge can be experimentally gained, tackled by diverse complementary Surface Science techniques, such as IR[1] or X-ray Photoemission (*XPS*) spectroscopies,[2] or the Scanning Tunnelling Microscopy (*STM*),[3] to cite a few. However such techniques suffer from inherent technical limitations and inaccuracies, plus often deliver averaged information. Thus, during the last decades it has been growingly popular to extract such atomistic information from accurate simulations run on suited models, where Density Functional Theory (*DFT*) applied on surface slab models have excelled over other approaches, being an excellent compromise in between accuracy and computational cost. Previous DFT studies on the adsorptive landscape on Transition Metals (*TMs*) have mostly focused on face-centred cubic (*fcc*) crystalline structures only,[4-6] while comparing, when possible, to detailed experimental information.

However, the trends one can withdraw from *fcc* TMs are limited, as all of them are grouped on the right part of the *d* series of the Periodic Table, see Figure 1, making that the gained trends could not be completely applicable on the full *d* block, with the concomitant problematic of extrapolating results. Because of this, the present project aims at solving this issue by examining the hexagonal close-packed (*hcp*) TMs, profiting from the fact that such TMs are well dispersed along the *d* block, being some located at the left, middle, and right parts, and thus

allowing, on one hand, to better represent, together with *fcc* results, the majority of TMs, plus, on the other hand, allowing interpolation of the obtained trend rules.

21 **Sc** Scandium hcp	22 **Ti** Titanium hcp	23 **V** Vanadium bcc	24 **Cr** Chromium bcc	25 **Mn** Manganese bcc*	26 **Fe** Iron bcc	27 **Co** Cobalt hcp	28 **Ni** Nickel fcc	29 **Cu** Copper fcc	30 **Zn** Zinc hcp
39 **Y** Yttrium hcp	40 **Zr** Zirconium hcp	41 **Nb** Niobium bcc	42 **Mo** Molybdenum bcc	43 **Tc** Technetium hcp	44 **Ru** Ruthenium hcp	45 **Rh** Rhodium fcc	46 **Pd** Palladium fcc	47 **Ag** Silver fcc	48 **Cd** Cadmium hcp
57 **La** Lanthanum dhcp	72 **Hf** Hafnium hcp	73 **Ta** Tantalum bcc	74 **W** Tungsten bcc	75 **Re** Rhenium hcp	76 **Os** Osmium hcp	77 **Ir** Iridium fcc	78 **Pt** Platinum fcc	79 **Au** Gold fcc	80 **Hg** Mercury other

Figure 1: The *d* block of the Periodic Table showing the TMs from groups III to XII. The *fcc*, *hcp* and body-centered cubic (*bcc*) TMs are shown shadowed in blue, light green, and light brow, respectively.

On the *fcc* TM surfaces, the CO adsorption has been already well-studied and characterized, so that the CO interaction with surface metal atoms is known to be through the C atom, with the molecule bond positioned perpendicular to the metal surface, as observed on most stable, low Miller indices, (001), (011), and (111) surfaces, although the interaction can occur on different surface positions, typically top, bridge, or hollow positions, depending on the metal and the exposed surface, also following the type of connectivity as obtained when attaching CO to metal dimers[7,8] or small metal clusters.[9,10] Here the intention is to carry out the same thorough sampling on the low Miller indices surfaces of *hcp* TMs of order one, including the (0001), (10$\bar{1}$0), and (11$\bar{2}$0) surfaces, see Figure 2 —surfaces notation is described later.

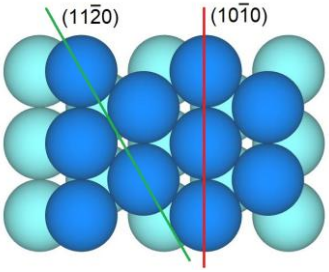

Figure 2: Top view of a (0001) *hcp* surface, where lines define the vertical (10$\bar{1}$0) and (11$\bar{2}$0) surfaces. Surface and first subsurface metal atoms are shown as dark and light blue spheres, respectively.

One has to stress that atomically resolved data on CO adsorption could be experimentally determined, although such studies need to have well-characterized single crystal metal surfaces, to dose CO in a controlled fashion using a vacuum chamber, while controlling the pressure and temperature conditions. As one could easily think, such experiments, yet feasible, are by no means easy, and some properties require having highly sophisticated apparels, such as STM to estimate molecular heights, X-Ray Diffraction (*XRD*) *e.g.* to estimate bond lengths, and microcalorimetry experiments to estimate adsorption energies. Aside, one has to keep in mind that, on some metals, or even some surfaces of a given metal, the CO adsorption can be irreversible, reacting with the TM or being its decomposition catalysed by it, thus eventually jeopardizing the analysis.

As aforementioned, such technical drawbacks limit the acquisition of information, which can luckily be easily gained by computational calculations, though, normally being DFT the nowadays working horse. Such computations have been extensively used to accurately describe the interaction of atoms and molecules on surfaces, and the reactivity among them.[11-13] By DFT means, applied on proper surface models, one can easily determine the adsorption strength and conformation, geometric parameters, even allowing the simulation of IR spectra of the adsorbed molecule. Here we will exploit such in describing, in an exhaustive and thorough manner, the interaction of CO on the aforementioned TM surfaces, acquiring thus different geometric, energetic, electronic, and vibrational features including CO bond lengths, d(CO), the height of the CO molecule with respect the surface, h, the adsorption energy, E_{ads}, and the CO bond stretching vibrational frequency, ν(CO), while evaluating the suitability possible descriptors argued in the literature, such as the d-band centre, ε_d,[14] or the surface energy, γ, [15] and examining, yet in a gross fashion, the trends over CO breakage.

4. OBJECTIVES

The main goal of this project is to evaluate the CO adsorption trends on TM surfaces. To do so, the most stable adsorption interaction, including different conformations, will be analysed on the most-stable low Miller index (0001), (10$\bar{1}$0), and (11$\bar{2}$0) surfaces by carrying out accurate DFT calculations on suited surfaces slab models. The interaction will be analysed from the geometric, energetic, electronic, and point of views. The specific goals of the study are thus:

- To validate the employed DFT methodology consistency comparing the presently obtained data with previously estimated ones as available in the literature.
- To sample the CO adsorption in a thorough manner so to ascertain the most stable position for CO on each studied TM and surface.
- To estimate the bias of possible geometric, energetic, and electronic descriptors on the CO adsorption across the studied systems.
- To correlate or analyse the CO bonding based on the estimated descriptors.
- To investigate the possible CO irreversible breakage when adsorbed.
- To simulate the IR spectrum of the most stable positions of each surface and evaluate the possible correlation of the IR CO stretching position and intensity with the CO bonding and conformation.

5. THEORY

This section aims at providing, in a brief fashion, some information of the underlying theory employed in the calculations to facilitate the understanding. Because of the limits, this information is given in a succinct and applied way, mostly addressed at the studied CO adsorption process, rather than on a deeply and mathematically sound fashion, for which we refer to the literature.

5.1. SCHRÖDINGER EQUATION

Quantum chemistry grounds in the principle that in every instant a chemical system is defined by a wavefunction, Ψ. By applying an operator —a mathematical formula— to it, the exact value of a given desired property of this system can be obtained. One of the properties sought for every system is its total energy, *E*, which can be determined by applying the Hamiltonian operator, $\hat{\mathrm{H}}$, onto the wavefunction, following the Schrödinger equation:

$$i\hbar\frac{\partial\Psi_t}{\partial t} = \hat{\mathrm{H}}\Psi_t \qquad \text{(Eq. 1)},$$

where ħ is the reduced Planck constant, and Ψ_t the time-dependent wavefunction. The normal simplification is that the system energy is constant during the pass of time, with the well-known time-independent Schrödinger equation:

$$\hat{\mathrm{H}}\Psi = \mathrm{E}\Psi \qquad \text{(Eq. 2)}.$$

The Hamiltonian can be divided in several terms: two kinetic operators, $\hat{\mathrm{T}}$, and three coulombic energy operators, $\hat{\mathrm{V}}$:

$$\hat{H} = \hat{T}_n + \hat{T}_e + \hat{V}_{nn} + \hat{V}_{ee} + \hat{V}_{ne} \qquad \text{(Eq. 3)},$$

where $\hat{T}_n$ and $\hat{T}_e$ represent the kinetic energy of nuclei and electrons, respectively, while $\hat{V}_{nn}$ is the coulombic repulsion between nuclei, $\hat{V}_{ee}$ the repulsion between electrons, and $\hat{V}_{ne}$ the attraction between nuclei and electrons.

To solve this equation it becomes practical to use the Born-Oppenheimer (*BO*) approximation. This approximation relies in the fact that the mass of the nuclei is much larger than that of the electrons, so that their motion can be treated separately. This implies that the $\hat{T}_n$ could be simplified as zero and $\hat{V}_{nn}$ would become a constant. When these two values are neglected the electronic Hamiltonian can be defined as:

$$\hat{\mathrm{H}}_e = \hat{T}_e + \hat{V}_{ee} + \hat{V}_{ne} \qquad \text{(Eq. 4)},$$

and applied to the wavefunction to get the electronic energy. The application, though, is neither immediate nor exact, as the wavefunction is normally unknown and has to be approximated and optimized, where the basics of the wavefunction approximation and the energy optimization can be found in the Hartree-Fock (*HF*) method, seed of other improved methods contained in the so-called post-HF methodologies. The principal issue of HF and post-HF methods is that, even when the results are accurate, their required computational cost can be very high, making some simulations hitherto still unaffordable. Because of this some alternative methods were developed, being a good compromise in between accuracy and computational cost; we explicitly refer here to DFT, which is explained next.

5.2. DENSITY FUNCTIONAL THEORY

The Density Functional Theory (*DFT*) is one of the alternative methods to the wavefunction methodologies, and one of the most popular ones, specially given its comparatively lower computational cost. DFT is based in the postulate that the energy of a polyelectronic system only depends of the electron density function, $\rho(\mathbf{r})$, which depends only on the electron density coordinates, **r**. Thus, it does not need to know the wavefunction of the system, for which one would need to define and handle 3N coordinates —being N the number of electrons of the system. Since the electron density function only has three coordinates —actually four when the spin is included— the calculations get very simplified. Furthermore, there are two theorems —the Hohenberg-Kohn theorems— that back up the basis and use of this method.

5.2.1. First Hohenberg-Kohn Theorem

In 1962 Pierre Hohenberg and Walter Kohn published their two famous theorems.[16,17] The first theorem showed that for an electron density of the ground state, $\rho_0(\mathbf{r})$, there is only one possible external potential, V_{ext} (**r**), that defines it. This implies that the electron density is

determined by the external potential, and *vice versa.* This would mean that, with a known electron density, the nuclei positions could be determined. As a corollary this theorem states as well that the energy is a function of the electron density function, this is, a functional.

$$\rho_0(\boldsymbol{r}) \Leftrightarrow V_{ext}(\boldsymbol{r}) \quad \text{(Eq. 5)},$$

$$E = E[\rho_0(\boldsymbol{r})] \quad \text{(Eq. 6)}.$$

5.2.2. Second Hohenberg-Kohn Theorem

The second Hohenberg-Kohn theorem deals with the optimization of the system. It postulates that the electron density that minimizes the energy functional is that of the ground state, delivering the ground state energy, E_0, and that any other density would deliver a higher energy. There are different ways of demonstrating this theorem, and one of the most popular ones is a reduction *ad absurdum*. For more details, we refer to the literature,[16,17] but the ground idea is that this theorem serves as the safety net to optimize the electron density towards that of the ground state, as done in the Kohn-Sham method, explained next.

$$E_0[\rho_0(\boldsymbol{r})] < E[\rho(r)] \quad \text{(Eq. 7)}.$$

5.2.3. Kohn-Sham Method

The Kohn-Sham method describes the process to minimize the electron density of a given system. For that, the developers helped themselves using a reference system made of a homogeneous gas with no interactions between electrons. Aside, the authors stated that a polyelectronic system with a given density could be replaced by their system with non-interacting electron with the same density. This led to a splitting of the energy of the system into different terms:

$$E = T_s + E_{ext} + J + E_{xc} \quad \text{(Eq. 8)},$$

where T_s is the kinetic energy of the electrons of the system, E_{ext} the attraction between the electron density and the external potential, J the coulombic repulsion between electrons, and, finally, E_{xc} is the difference between the real system and the one with no electronic interaction. From these terms only the last one, called exchange-correlation functional, E_{xc}, has not been successfully defined yet, and so, has been approximated in different manners, from very simple to more complex ones. Actually, the development of exchange-correlation functionals is a field of research by itself, and is briefly explained next.

5.2.4. Exchange and Correlation Functionals

The issue that has become a rock-in-the-shoe in the use of DFT is the exchange-correlation (*xc*) functional. For this reason many research endeavours were applied in order to define it. They were classified in the so-called Jacob's ladder, where each step represents a different level of *xc* definition and improvement.

The lowest rung of the ladder is known as the Local Density Approximation (*LDA*), which assumes that the density only depends on the coordinates. The second one is the Generalized Gradient Approximations (*GGA*), where the functional does not only depend on the electron density at each point but also depends of the density gradient. Next are the Meta-GGA functionals, which now include also the second gradient of the density. Finally, one of the highest steps is the hybrid methods, which include some portion of HF exchange energy in their calculations. Notice that other higher rungs have been appointed, including exact exchange functionals. For more information about them, we refer to the literature.

The *xc* that has been chosen for this project is one within the GGA family, which is the second rung of the ladder. This rung has been found to be the best choice in describing TMs bulk and surfaces,[18,19] especially the PBE *xc* functional, the one chosen for this project, as functionals of higher rungs start impoverishing the delocalized electronic structure of TMs by localizing the electronic states.[20]

5.3. CRYSTALLINE STRUCTURES

A crystalline structure is one where all the atoms are ordered following a regular pattern known as unit cell. They form a basic crystal lattice that extends in the three dimension of the space. Each structure has a representative primitive unit cell, which is the one with lowest volume that is repeated through the structure. The unit is defined by three lattice vectors that form it, $\vec{a}_n$, and the angles among them. The modules of the vector and the angles between them are known as the cell parameters, and the relations between them are used to define the different types of cells. For example, the *hcp* structure is an hexagonal unit cell with ABA layer stacking. The relation between its parameters are $\mathbf{a}_1 = \mathbf{a}_2 \neq \mathbf{a}_3$, $\alpha = \beta = 90°$ and $\gamma = 120°$ or $60°$, depending on where the origin of coordinates is taken, see Figure 3.

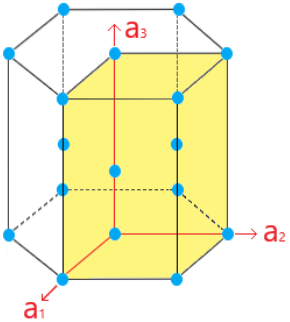

Figure 3. View of an *hcp* crystal structure with the primitive unit cell shaded in yellow. Each dot represents an atomic position. The three lattice vectors are shown in red.

5.3.1. Reciprocal Space

The reciprocal lattice is the projection of the direct lattice in another space by using a Fourier transform. The module of the new vectors can be calculated through the next equation:

$$\boldsymbol{b_i} = 2\pi \frac{\boldsymbol{a_j} \times \boldsymbol{a_k}}{\boldsymbol{a_i} \cdot (\boldsymbol{a_j} \times \boldsymbol{a_k})} \; \forall_{i,j,k} \in \{1,2,3\} \qquad \text{(Eq. 9)},$$

where, perhaps, the most illustrative thing to see is that the module of the reciprocal vector is inversely proportional to the direct one, meaning that the larger is the direct cell, the smaller the reciprocal cell will be. The importance of the reciprocal cell resides in the type of calculations, being periodic. As a consequence of the Bloch theorem,[21] imposing translational symmetry to the unit cell, it happens that the wavefunctions have a component in this reciprocal space, and so the operations are often treated in such a space.

Regardless of this, one has to keep in mind that there are still infinite points within the reciprocal unit cell, and so it is impossible to handle the electronic states in infinite points. Thus, normally one defines a finite number of points in the reciprocal space where to calculate the electronic states, the so-called **k**-points. A typical choice is to create a mesh so as to divide the space in equal parts, and calculate in the **k**-points defined at the nodes of the mesh. As one can intuitively understand, the denser is the mesh, the better the description is; aside, on a small direct cell, and so, a large reciprocal cell, more **k**-points will be needed to get accurate and converged results, while in the opposite case only fewer points would be needed, up to the point of only one single point, called $\boldsymbol{\Gamma}$, for isolated systems as could be molecules in vacuum.

5.3.2. Miller Indices

Crystal planes can be represented with three values or indices —four in the case of hexagonal cells— which are (*hkl*) —or (*hkil*)—, called Miller indices. These values represent a vector ***g*** that, as a basis on the reciprocal cell, can be defined as:

$$\boldsymbol{g_{hkl}} = h\boldsymbol{b_1} + k\boldsymbol{b_2} + l\boldsymbol{b_3} \quad \text{(Eq. 10)},$$

where the vector is perpendicular to the defined plane. Another easier way to interpret the three values can be done on the direct cell, looking where the plane intercepts the direct cell vectors. Each letter represents a point of interception that is in the same direction as that vector, and the index value is how many times is distanced from the origin of coordinates referred to the module of the vector. The represented plane is the one that has all three points of interception. If the plane is parallel to the vector and does not intercept the vector, then its value is 0, see examples of such in Figure 4.

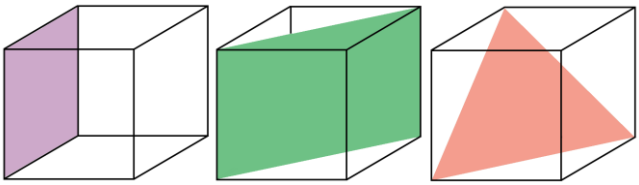

Figure 4. View of a cubic cell where the (010), (110), and (111) surfaces are marked in purple, green, and pink, respectively.

In an hexagonal cell, the *i* index is auxiliary, and is a value that does not give any new information about the plane, yet fulfils the next equality:

$$i = -(h + k) \quad \text{(Eq. 11)},$$

This *i* index value is necessary to carry out a permutation between indices. In cubic-like systems, vectors are naturally orthogonal among themselves. However, since the three vectors that define the three-index Miller indices in hexagonal-like crystal structures are not orthogonal, that creates a problem with the *hcp* structures in terms of mathematical projections. When the fourth index is added, one can permute vectors, so that they can be orthogonal, see Figure 5.

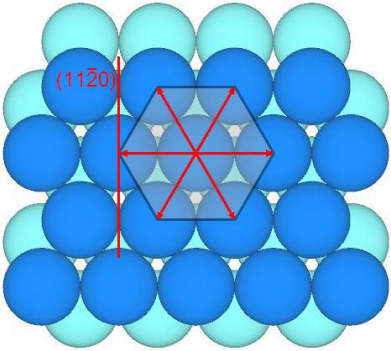

Figure 5: View of a (0001) surface marked with all equivalent directions of (10$\bar{1}$0) surfaces and a (11$\bar{2}$0) case for an *hcp* structure.

In any case, the Miller indices can be positive or negative, but have to be integers numbers. Furthermore, they must have a greatest common divisor of one. This is due to the fact multiple planes are represented by the same direction, and are equivalent and parallel. The planes that we are going to study are the ones with a maximum Miller index order of one; the (0001), (10$\bar{1}$0), and (11$\bar{2}$0), see Figure 6.

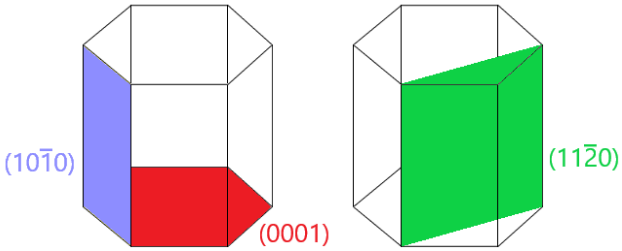

Figure 6: Views of the studied *hcp* planes, colour tagged.

5.3.3. Slab Model

In order to study a periodic surface there are some things needed to be taken into consideration. One is to account for a model which would enable assessing the surface energetic creation and its relaxation. Normally, the slab model is the most popular one when studying surfaces within Periodic Boundary Conditions (*PBC*). It consists of a number of atomic layers, where the bottom ones are normally kept fixed to simulate the material bulk, while the top ones are able to relocate or relax in the presence of vacuum or species upon, see Figure 7. In this study we employ 6-layered slab models, relaxed as a 3+3, which means that there are

three bottom layers of fixed atoms, while the three upper ones can relax during the optimizations.

As above stated, such slabs are contained within PBE, and so, a cell is defined, so that the slab is periodic along the modelled surface, as well as perpendicular to it; however here a vacuum region is added, to prevent any interactions between periodically repeated slabs. Normally, a distance of the vacuum of 10 Å is well enough to avoid such interactions, or to be regarded as negligible, at least.

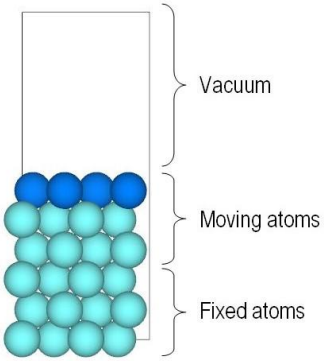

Figure 7: Side view form a slab model with its parts indicated, being surface layer coloured dark blue, and the inner layers shown in light blue. Frozen and relaxed parts are pointed out.

5.4. ADSORPTION

Adsorption is the process of interaction of an atom, ion, or molecule, called hereafter adsorbate, with a solid surface, called from now on substrate. There are normally two types of adsorption depending on its strength: physisorption or chemisorption. When there is a physisorption type, there is a weak interaction between the surface and the adsorbate, *e.g.* when driven by dispersive forces, as Van der Waals type of interactions, whereas in the chemisorption the interaction is much stronger and normally a new bond is created and can be claimed. The strength of the adsorption can be quantified by the adsorption energy, defined by the difference of the adsorbed system energy with respect the free adsorbate and the pristine surface.

$$E_{ads} = E_{AS} - (E_A + E_S) \qquad \text{(Eq. 11)},$$

This E_{ads} is thus defined negative, and the more negative the value the stronger the adsorption. This energy can be used to classify the type of undergone adsorption, as in the case

of physisorption the adsorption energies are relatively small —*e.g.* ranging from 0.01 to 0.3 eV— while chemisorption has larger adsorption energies —normally above 1 eV. This classification is not strict, though, and should be regarded as qualitative, as a weak interacting system with many contact points can add up the adsorption strength below -1 eV.[22] On the other hand, a bond can be created, but repulsions may counteract the adsorption strength, pulling it above -1 eV.[23]

5.4.1. Donation and Back-Donation

The adsorption of the CO on *hcp* metals, and on most of *fcc* metals, is known to be a chemisorption.[24] The new bond is typically formed following a donation/back-donation electron density mechanism between the CO and the surface metallic atom to which is bonded to. First, the CO molecule, through its C atoms, gives electron density from the Highest Occupied Molecular Orbital (*HOMO*) to the metal surface atom forming a σ bonding, which is regarded as the donation process, see Figure 8. At the same time, this surface metal atom is giving electron density back to a π^* antibonding orbital of the CO molecule, which is regarded as the back-donation process, see Figure 8. The occupation of an antibonding orbital has a direct consequence in the strength of the C-O bond, which weakens, enlarges, and features a smaller stretching vibrational frequency.[25]

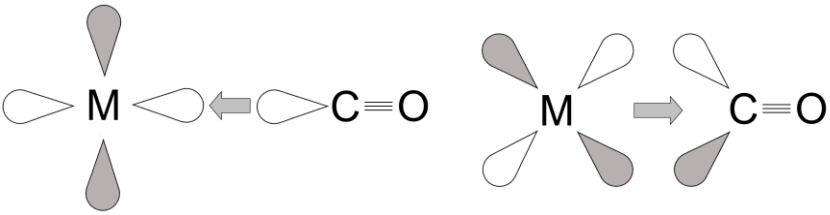

Figure 8: Representation of the orbitals involved in the donation process (left) and back-donation process (right).

5.4.2. Adsorption Sites

The CO molecule can attach over three different types of sites depending on the number of surface atoms it interacts with. For instance, CO can adsorb perpendicular and interacting with a single metal atom, *i.e.* on top (T) of a surface metal atom, or on a bridge (B) position connecting to two vicinal metal surface atoms, or over three or more atoms over a hollow (H) site. On a given surface there is the possibility that there are more than one topologically

different bridge or hollow positions, which consequently requires labelling them differently. For instance, differentiating the bridge length —bridge long (B_L) or bridge short (B_S) positions— or whether there is or not an atom beneath a hollow —basic hollow or hollow empty (H_E)—, see Figure 9. At the same time, the adsorption of the CO could be in a parallel fashion; in this case, the notation gets more complicated. The list of sampled conformations is shown in Figure 9.

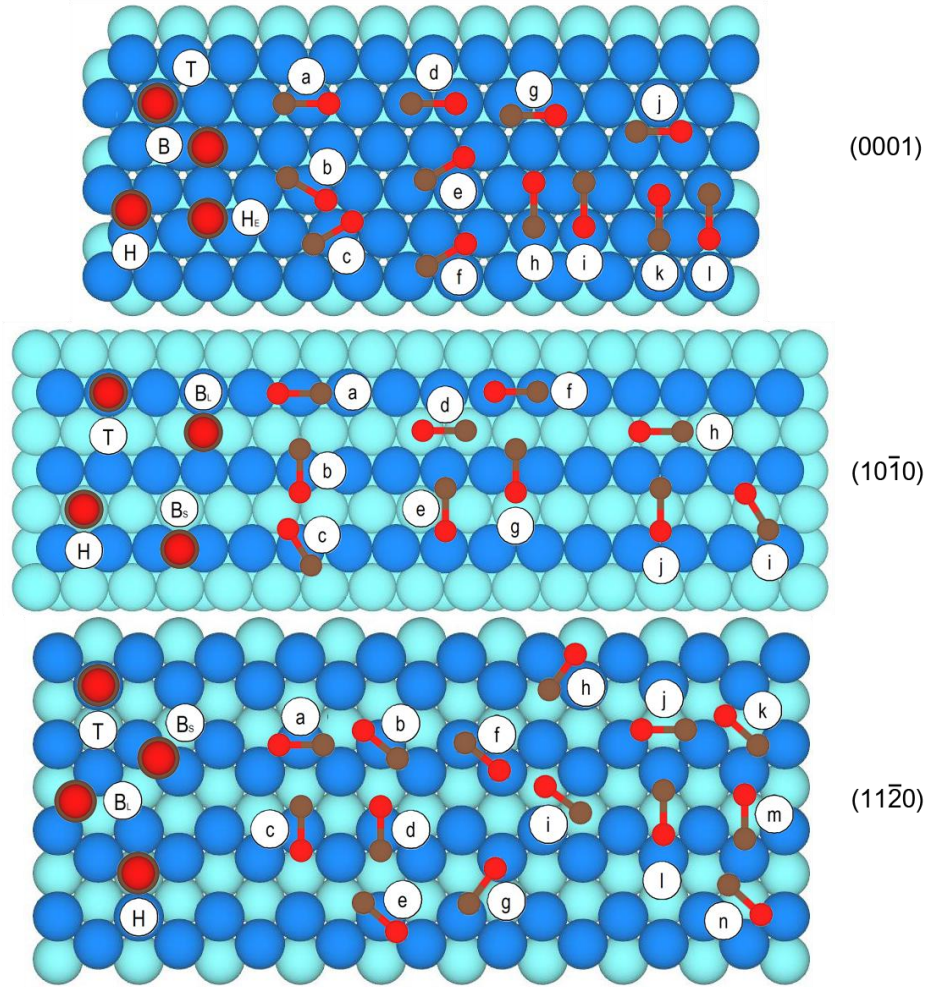

Figure 9: Top views of the studied CO positions on the considered surfaces. Molecules on the left belong to perpendicular positions, labelled on the C atom position. The ones at the middle and right are labelled with a letter. Colour code as in Figure 7, with C and O atoms as brown or red spheres, respectively.

Regardless of the initial position, and whether the CO is placed perpendicular or parallel, the CO was initially always located approximately 2 Å over it the site. Notice that, as there are no constrains in the optimizations, a CO molecule can change its conformation and position during the optimization process.

5.4.4. Supercell

When an adsorption process occurs there is a chance that there is an interaction between adsorbates located close to each other over the surface. For this study this interaction needs to be minimized as we want to study such a process on the cleanest, simple situation belonging to a low CO coverage, so as to avoid lateral interaction effects that would complicate the analysis. Even when carrying out simulations with a single CO molecule on a periodic cell, one has to regard that such a system is periodically repeated, where the molecule can interact with the other translational images of itself. The use of a relatively small unit cell may provoke that the CO molecules can effectively interact. To avoid this, a supercell is used, where the basic unit cell is multiplied a certain amount of times, gathering a few units, see Figure 10. This expanded unit cell would make the distance between molecules longer, thus preventing an eventual significant interaction. Such supercells are normally named as the number of repetitions on each direction. In this case, the replication is going to occur on direction $\mathbf{a}_1$ and $\mathbf{a}_2$, which means that there is only the need of two numbers. For the surfaces (0001) and $(11\bar{2}0)$ the supercell is going to be (2×2) while for $(10\bar{1}0)$ a (3×3) is used, so that the different employed supercells have comparable number of surface metal atoms of eight or nine.

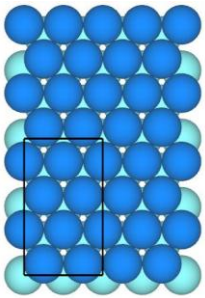

Figure 10: Top view of an orthogonal (0001) supercell (2×2) where the original unit cell is contoured with black lines.

5.5. VIBRATIONAL FREQUENCIES

The IR spectroscopy is a widely used technique where a system absorbs infrared radiation, normally getting vibrationally excited. The intensity of the vibration for an adsorbed molecule is experimentally said to be determined by the empiric surface dipole selection rule applied on an active vibrational model. At variance with spectroscopic selection rules, the surface dipole has an empiric origin, and is stated as that one vibrational mode is active when it has associated a change in the molecular dipole moment. When we deal with an adsorbate, like the adsorbed CO, the metal surface electron density can generate a mirror dipole to that of the molecule, which can affect the total dipole. When the dipole of the molecule is perpendicular to the surface, the surface dipole adds to it, and so the vibration mode would be IR active, see Figure 11. However, when the dipole of the molecule is parallel to the surface, the opposite dipole may counteract it provoking that the vibration mode is not active, being an IR invisible ghost mode, see Figure 11. In general terms, this is reduced at having the vibrational mode (or bond) being perpendicular or parallel to the surface. This selection rule can be easily hypothesized when having dimer molecules; but notice that when having a polyatomic molecule, the coupling in between vibrations has to be taken into account, as such can provide a change in the dipole moment perpendicular to the surface for a bond which is parallel, as seen *e.g.* in the propyne adsorption on Cu(111).[26]

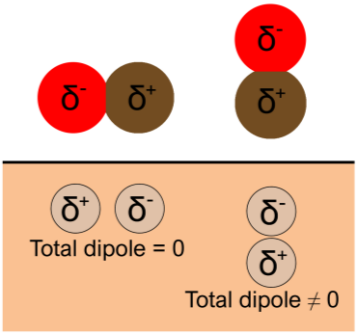

Figure 11: Representation of the CO molecule adsorbed on a surface in a parallel (left) and perpendicular (right) conformations the respective dipoles and surface image mirror dipoles.

6. COMPUTATIONAL DETAILS

All present DFT calculations have been done using the Vienna *Ab initio* Simulation Package (*VASP*),[27] using the PBE *xc* functional,[28] known to be among the best GGA functionals in describing TM bulk and surface properties.[18,19] Notice that no dispersive forces correction has been applied, even though such can contribute by a constant value of *circa* 0.2 eV to the CO adsorption,[29] but such a decision has been used to profit from C and O adsorption energies as previously calculated at PBE level.[30,31] The *hcp* TMs (0001), ($10\bar{1}0$), and ($11\bar{2}0$) surfaces were modelled using (2×2) supercells, except for the ($10\bar{1}0$) which was a (3×3), which ensures having a similar number of surface metal atoms of eight or nine, and so, a similar coverage. Each of the used slab models consists of six atomic layers and a minimum 10 Å vacuum region on top of them. The three bottom layers were fixed to emulate the bulk environment, while the three top layers were able to relax —*i.e.* 3+3 approach—. To sample the reciprocal space, an optimized Monkhorst-Pack **k**-point mesh of 3×3×1 dimensions has been used, as proven in the past to deliver results converged below the chemical accuracy of 1 kcal·mol^{-1} —~0.04 eV.[32]

The geometry optimizations have been carried out with a plane wave basis set with an energy cutoff of 415 eV, also enough to reach the chemical accuracy of ~0.04 eV. Energetic optimization criteria of 10^{-5} and 10^{-6} eV have been used for the atomic and electronic steps. All calculations have been carried out non-spin polarized except for the magnetic Co surfaces. To describe the core electron density, Projector Augmented Wave (*PAW)* pseudopotentials have been used as recommended by VASP developers.[33] The isolated CO molecule has been optimized likewise but isolated in the centre of a large unit cell of 10×10×10 Å dimensions, and carried out at Γ point, and the same was used for isolated C and O atoms, isolated in cells of 9×10×1º Å dimensions to force correct orbital occupancy. The vibrational frequency calculations were carried out for the CO molecule decoupled from the surface phonons, and performed by finite differences of 0.03 Å in length, thus building and diagonalizing the Hessian matrix, while adding a counterdipole in the middle of the vacuum region to assess the variations of the dipole moment due to the CO adsorbate vibrations.

7. RESULTS AND DISCUSSION

7.1. METHOD VALIDATION

To validate whether the results are consistent or not they have been compared to previous DFT values.[34] Notice that, in the literature, such results were gained using as well slab models, yet not always with the same number of layers, vacuum, degree of relaxation, cutoff, and **k**-point meshes. Aside, those were previously obtained using the RPBE[35] and PW91[36] *xc* functionals, that, even being GGA ones and so close to the current PBE, can lead to some variations. The comparison used comprised E_{ads} values of CO on positions η^1-CO-μ^1-C_T, η^1-CO-μ^1-C_B, η^1-CO-μ^1-C_H, and η^1-CO-μ^1-C_{H_E} on the (0001) surface of Co, Re, and Ru, plus the η^1-CO-μ^1-C_T position on the (0001) surface of Zn —the site labelling is fully explained in the next section. To make a fair comparison, we correlated PBE results *vs.* PW91 or RPBE, see Figure 12.

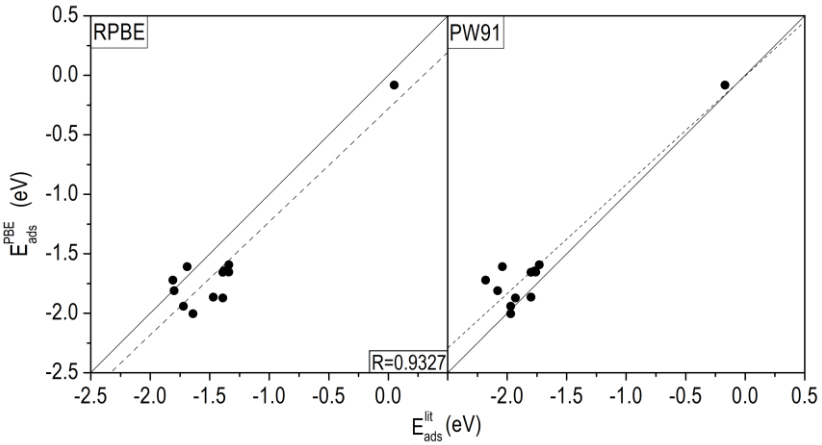

Figure 12: CO adsorption energies as here obtained using the PBE *xc* compared to previous literature (lit) estimations using the PW91 or RPBE *xc* functionals. The dashed line represents the adjustment, whose formula and regression coefficients are shown.

Notice that in both cases the result are very similar to the obtained ones here by PBE, and the trend is captured, with only a systematic shift of PBE being ~0.4 eV stronger than RPBE and

comparable to PW91, a natural result given the similitude of PBE and PW91 when simulating TM systems.[19] Such a comparison has to be taken with a grain of salt, as the results from other TMs and surfaces are missing, as well as comparison with experiments. So, with the limited amount of data, what we can claim is that the same adsorption strength trends are found either using PBE, PW91, or RPBE *xc* functionals, although a clearer statement would need more calculations on other TMs and surfaces, and, actually, a better assessment would be obtained with respect experimental results, unfortunately, not available yet.

7.2. CO FINAL POSITIONS

7.2.1. Site labelling

Having defined that the computing level is adequate to capture trends, we explain here the labelling of the explored sites. The obtained CO adsorptive minima have been classified by the location of each of the atoms following a coordination chemistry notation. Thus each of them has been referred with a tag that unequivocally differentiates it form others. This tag is simply explained as:

$$\eta^{a}\text{-CO-}\mu^{b}\text{-}\ C_1O_2$$

where *a* is the number of atoms of the CO molecule interacting with the surface, *b* the number of atoms of the surface interacting with the CO, and *1* and *2* the positions the C and O atoms occupy, respectively. As an example, η^2-CO-μ^2-$C_{B_S}O_T$ on the $(10\bar{1}0)$ surface, see Figure 13, implies the two atoms of CO molecule interacting with two metal surface atoms, so that the C is located over a B_S site, while the O atom is placed directly on-top of one such metal surface atoms. At full list of labels is shown in the Appendix 1 for (0001), $(10\bar{1}0)$, and $(11\bar{2}0)$ surfaces, respectively, and correlated with the simplified labelling in Figure 9.

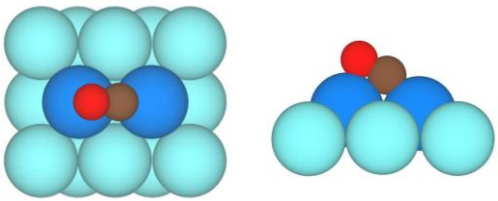

Figure 13: Top and side view of a CO molecule positioned on η^2-CO-μ^2-$C_{B_S}O_T$ on a $(10\bar{1}0)$ surface.

7.2.2. New positions

In this section we address the obtaining of new, previously unforeseen adsorption sites, while the initially explored ones are next fully tackled in section 7.2.4. On the close-packed (0001) surface no new positions were found, although this actually did happen on the $(10\bar{1}0)$ and $(11\bar{2}0)$ surfaces. Particularly on the $(10\bar{1}0)$ surface two new positions were found which could be classified as Hollow sites, although in both cases there are interactions with the subsurface atoms. When one of the CO atoms interacts with one subsurface layer metal atom and simultaneously two surface layer metal atoms the position is referred hereafter as Hollow – 2 Top (H_{2T}), see Figure 14, whereas when it is interacting with two subsurface layer metal atoms and only one surface layer metal atom this is catalogued as Hollow – 2 Bottom (H_{2B}), see Figure 14. Notice that these can be regarded as displaced B_S and T sites, respectively. Aside, the original B_L position can change due to the fact that the atom on that position lowers its height as much as to interact with the subsurface metal atoms. This position is referred from now on as Bridge Long – Low (B_{L_L}), see Figure 14. This position is more stable than B_L, causing that there were actually no atoms found in the B_L strict position.

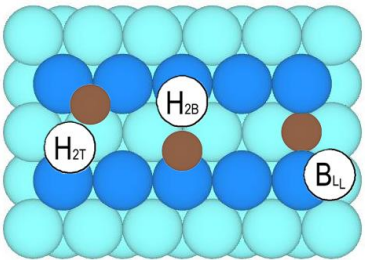

Figure 14: Top view of $(10\bar{1}0)$ surface with atoms on the new positions, alongside with their respective labels. Colour coding as in Figure 9, with position exemplified here with C atoms, while could be occupied by O atoms.

On the $(11\bar{2}0)$ surface, two of such positions were also found; the so-named H_{2T} and B_{L_L}, see Figure 15. Aside, two new further adsorption sites appeared. These positions are both catalogued as a Bridge, but involving a surface and a subsurface metal atom. When there are no side surface atoms, the position is similar to a B_S position but tilted, referred from now on as B_S diagonal (B_{SD}), see Figure 15. On the other hand, when there are side atoms, this becomes similar to a B_L position, and so is referred hereafter to as B_L diagonal (B_{LD}), see Figure 15.

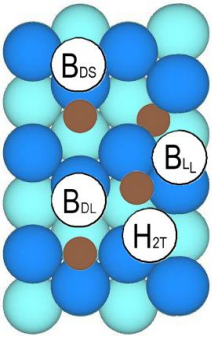

Figure 15: Top view of of (11$\bar{2}$0) surface with atoms on the new positions, alongside with their respective labels. Colour coding as in Figure 9, although keep in mind that event though here the position is exemplified with C atoms, while could be occupied by O atoms.

7.2.3. Reconstructions

When the CO adsorbs on a surface, it unavoidably suffers some sort of bond length change. Such a distortion could be so insignificant so as to be negligible. Furthermore, not only the CO molecule can modify its geometry, but the surface itself can deform; either along the vacuum direction, called relaxation, or along the surface direction, called reconstruction. In the explored cases, such relaxation/reconstruction is observed, and the different surface geometries go back to the original conformation when CO desorbs, yet, in some cases, they do not, resulting in a new type of reconstructed surface. Such reconstructions often appear when allowing degrees of freedom using supercells, as here used, and a formal inspection would require studying different supercell sizes, which, unfortunately, falls out the computing capabilities and focus of the present study. The accounting of such reconstructions is vital, so as to properly size the E_{ads} values. Otherwise, such E_{ads} estimations would erroneously account for both the adsorption and reconstruction processes, typically unduly enlarging the E_{ads} strength, and provoking trend deviations. Next we summarize the types of observed reconstructions.

7.2.3.1. Squared reconstruction

This type of reconstruction is only observed on groups III and IV TM (11$\bar{2}$0) surfaces. As can be seen on Figure 16, there is a movement of half the atoms of a row towards a vicinal row, creating a pattern of pseudo squares over the surface, with angles of or near to 90º.

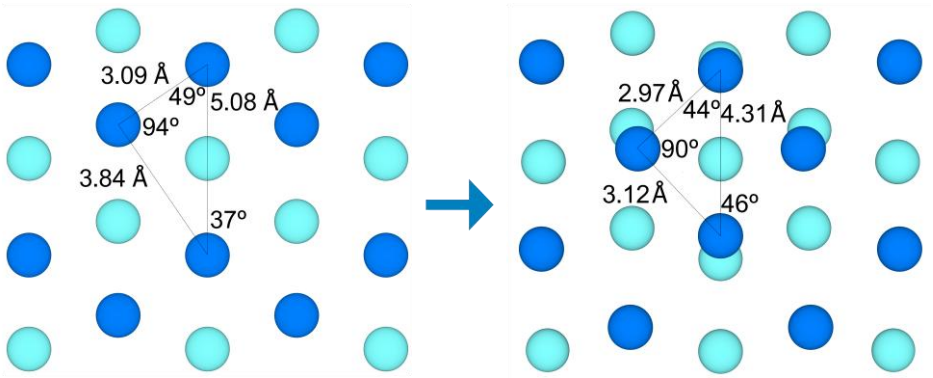

Figure 16: Representation of the relative positions of the atoms before (left) and after (right) the reconstruction, including illustrative surface metal bond lengths and angles. Colour coding as in Figure 9.

However, this surface is not stable *per se*, and so, recovers the original form when desorbing CO permitting relaxation back towards the original one. Thus, this reconstruction can be claimed to be CO-induced. This reconstructed surface also displays different adsorption sites, and so, there is technically no longer B_S or B_L sites, and so such are regarded as simple Bridges, B. Even though the reversibility of such a reconstruction, its DFT appreciation is of utmost importance, as experimentally one could, for instance, detect some sort of (001) square surface when having CO adsorbed, *e.g.* when studying it by X-ray Diffraction (*XRD*). Energetically, though, the change is minimal, with a surface energy decreases of *ca.* 0.02 $J \cdot m^{-2}$ from a surface energy of 1.26 $J \cdot m^{-2}$ for the Sc, 1.02 $J \cdot m^{-2}$ for Y, and 1.64 $J \cdot m^{-2}$ for Zr.[19] In the cases of Ti and Hf, no significant change of energy is detected. Notice that the closeness of such surface states succinctly implies that such arrangements can be easily adopted without much an energetic cost, so far the interaction of CO with them is strengthened.

7.2.3.2. (10$\bar{1}$0) reconstruction

On some (11$\bar{2}$0) surfaces of group XII TMs a distortion occurs, much larger than the previously commented one, which, at variance, does not recover when desorbing CO. In the case of Zn this reconstruction seems to lead to a surface which resembles the (10$\bar{1}$0) one, see Figure 17. Such a transformation would make sense as previous studies estimated (10$\bar{1}$0) surface, with a surface energy of 0.57 $J \cdot m^{-2}$, being sensibly more stable than the (11$\bar{2}$0) one, having a surface energy of 0.91 $J \cdot m^{-2}$.[19] In the case of Cd surfaces such a reconstruction is visible, yet not so acute. This can be biased by a larger steric repulsion being its radius larger,

but also the energetic driving force as aforementioned for Zn does not exist, being $(11\bar{2}0)$ surface, with an unreconstructed surface energy of 0.50 $J \cdot m^{-2}$ being more stable than $(10\bar{1}0)$ one, with a surface energy of 0.61 $J \cdot m^{-2}$.[19] As can be seen on Figure 18, in the case of Cd such a reconstruction the atomic rows become less edgy, yet not fully straight, although in some cases, linear and zigzag rows alternate.

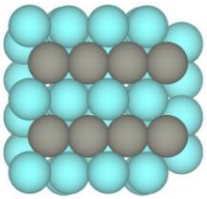

Figure 17: Top view of different possible reconstructions on a Zn$(10\bar{1}0)$ surface The dark pink spheres denote the reconstructed surface Zn atoms.

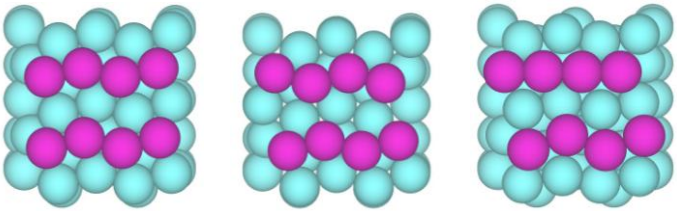

Figure 18: Top view of different possible reconstructions on a Cd$(11\bar{2}0)$ surface, including zigzag (left), alternate (middle), and one straight row (right) reconstructions. The dark pink spheres denote the reconstructed surface Cd atoms.

This process naturally implies that such reconstructed surfaces are more stable than the bulk truncated arrangements, and so, feature lower surface energies. The most acute case is for Zn, where the computed energy reduces by 0.20 $J \cdot m^{-2}$ compared to the bulk truncated one, as earlier computed to be of 0.91 $J \cdot m^{-2}$.[19] On Cd surfaces reconstructions with both rows still in zigzag feature a change of -0.06 $J \cdot m^{-2}$, while the one where one row alternates is of -0.03 $J \cdot m^{-2}$. The most acute reconstruction is when one row is fully straight, with a change of -0.10 $J \cdot m^{-2}$ with respect the computed value of 0.50 $J \cdot m^{-2}$.[19] Actually, such a surface reconstruction resembles a bit to the $(10\bar{1}0)$ surface, but slightly more stable —0.51 *versus* 0.61 $J \cdot m^{-2}$.[17] Aside, this diversity of patterns, all close in energy, seems to point out that such surfaces feature a surface liability, reminiscent of that of supported small metal clusters,[6] which can be translated into an easier

accommodation of species upon, up to the a presumably easier catalysis, fostered by a substrate that can easily deform and adapt to prompt the formation/breaking of bonds.

7.2.3.3. Circular reconstruction

There is one case that has been observed only on the $(10\bar{1}0)$ surface of Tc. When the CO is adsorbed, the surface metal atoms form two curves that embrace the adsorbed CO. This shape is not recovered when the CO is put apart, so it is a minimum in the potential energy surface. Actually, the reconstructed surface features two conformations topologically different depending on the relative positions of the curves; either can be facing each other or oval, see Figure 19.

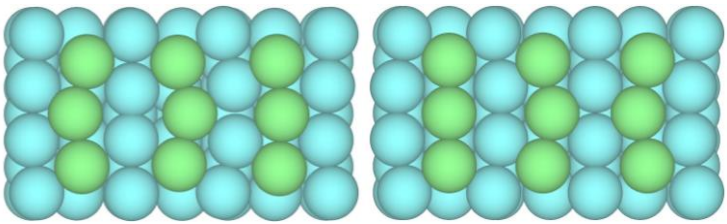

Figure 19: Top view of the two obtained conformations of a Tc reconstructed surface, including oval (left) and curve (right) reconstruction. The surface Tc atoms are shown as light green spheres.

The oval reconstruction has a change of surface energy of -0.24 $J \cdot m^{-2}$ with respect the computed value of 3.43 $J \cdot m^{-2}$ [19], yet close followed by the confronted one with a reduction of -0.21 $J \cdot m^{-2}$. Both of them thus significantly decrease the surface energy by reconstruction, but in proportion is not as accused as the aforementioned Cd and Zn cases. In any case, again, the energy closeness tends to think that such surface presents as well some sort of lability to accommodate or convert other chemical species upon.

7.2.4. Position trends

Having defined the new found sites and the effect of reconstructions, let us now analyse the positions trends. As far as they are concerned, one could first relate the number of atoms from the CO molecule that interact with the surface. Early TMs from groups III and IV are more likely to have both atoms interacting, *i.e.* η^2 situations, see Appendix 1. On the contrary, those of the groups VII to IX tend to interact only with the CO C atom, *i.e.* η^1 situations, where the contact is done over the slightly positively charged C, attracted by coulombic forces to the negatively charge surface metal atoms. Finally, the TMs from group XII usually do not feature any kind of

interaction. This can be seen both in general terms, or when focusing on most stable positions. This analysis reasoning can be extrapolated to the number of interacting atoms of the surface. When the two atoms of the CO molecule interact with the surface, there are more surface metal atoms participating in the adsorption, this is from μ^2 to μ^5, whereas for η^1 situations it goes from μ^1 to μ^4. As a rule-of-a-thumb, one could argue that, the larger the number of *d* valance electrons, the more likely is CO interaction solely through its C atom, which in turns goes with a larger negative surface charge, see Figure 20.

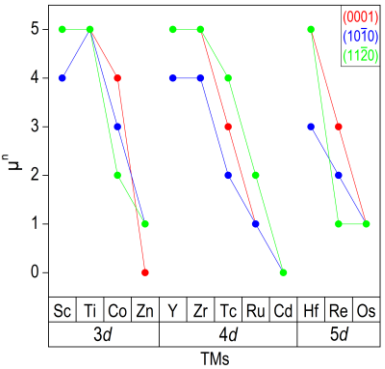

Figure 20: Graph representing the number of interacting atoms of each surface with the most stable position of the CO for each TM.

Looking down the groups there are also some trends; when going down a group — increasing the total number of *d* electrons— the CO tends to interact with less surface atoms at the same time. Even though this happens, the change is not as drastic as in a period. For example, comparing Ti and Zn one can see that CO does not adsorb on Zn in some cases while Ti does, interacting as well with the oxygen. However, Hf, located in Group IV, does still have most of the same final CO adsorption positions as in Ti, but with some more positions where CO oxygen does also interact. Again, this goes along with a larger radii down a group, and so, a more diluted electronic density, which thus becomes not so O-repellent, favouring the interactions with both atoms of CO.

7.3. STABILITY

Once the diversity of adsorption sites has been evaluated, we tackle now the stability, as analysed in terms of E_{ads}. The lower the energy, the more stable the adsorbed state is. Note that this energy has been taken regarding the possible surface reconstruction stabilization, *i.e.* the

newly found most stable reconstructed surface patterns have been taken as reference for the calculation of adsorption energies. With that into account, a series of trends can be withdrawn.

7.3.1. CO Position

The finally adopted positions seem to be a key contribution to the stability of the CO adsorption; as can be clearly seen in Table 1, with some clear trends relating the E_{ads} on the most stable CO positions. The E_{ads} thus can be related to the number of the interacting atoms of the surface, as those which have final positions with two contact points seem to be more stable; a point that also correlates with a lack of *d* electrons.

TM	(0001)		(10$\bar{1}$0)		(11$\bar{2}$0)	
	Label	E_{ads}	Label	E_{ads}	Label	E_{ads}
Sc	η^2-CO-μ^5-$C_HO_{H_E}$	-3.51	η^2-CO-μ^4-$C_{H_{2B}}O_{H_{2B}}$	-3.23	η^2-CO-μ^5-$C_HO_{B_S}$	-3.70
Y	η^2-CO-μ^5-$C_HO_{H_E}$	-3.14	η^2-CO-μ^4-$C_{H_{2B}}O_{H_{2B}}$	-3.06	η^2-CO-μ^5-$C_{B_{LD}}O_{B_{SD}}$	-3.55
Ti	η^2-CO-μ^5-$C_HO_{H_E}$	-3.39	η^2-CO-μ^5- $C_{BLL}O_{H(2T)}$	-3.33	η^2-CO-μ^5-$C_HO_{B_{SD}}$	-3.40
Zr	η^2-CO-μ^5-$C_HO_{H_E}$	-3.08	η^2-CO-μ^4-$C_{H_{2B}}O_{H_{2B}}$	-2.98	η^2-CO-μ^5-$C_HO_{B_{SD}}$	-3.39
Hf	η^2-CO-μ^5-$C_HO_{H_E}$	-3.22	η^2-CO-μ^3-$C_{H_{2T}}O_{B_S}$	-2.60	η^2-CO-μ^5-$C_HO_{B_{SD}}$	-3.23
Tc	η^1-CO-μ^3-C_{H_E}	-1.85	η^1-CO-μ^1-C_{B_S}	-1.77	η^2-CO-μ^4-$C_{B_L}O_T$	-1.68
Re	η^1-CO-μ^3-C_{H_E}	-2.00	η^1-CO-μ^2-C_{B_S}	-2.36	η^1-CO-μ^1-C_T	-1.72
Ru	η^1-CO-μ^1-C_T	-1.81	η^1-CO-μ^1-C_T	-2.15	η^1-CO-μ^2-C_{B_S}	-2.07
Os	η^1-CO-μ^1-C_T	-1.77	η^1-CO-μ^1-C_T	-2.28	η^1-CO-μ^1-C_T	-2.19
Co	η^1-CO-μ^4-C_H	-1.66	η^1-CO-μ^3-$C_{H_{2T}}$	-1.70	η^1-CO-μ^1-C_{B_S}	-1.76
Zn	—[a]	-0.28	η^1-CO-μ^1-C_T	-0.17	η^1-CO-μ^1-C_{B_S}	-0.27
Cd	—[a]	0.02	—[a]	0.10	η^1-CO-μ^1-C_{B_L}	-0.03

[a] **No interaction; possible physisorption**

Table 1: Position labels and E_{ads} of each of the most stable positions of CO adsorbed on each surface of each explored TM.

However, while comparing groups there is no big issue within a group, with few caveats. Down group IV the Zr does not line up on each surface. While on (10$\bar{1}$0) surface the E_{ads} is between those for Ti and Hf being in the same group, on the (0001) surface it becomes higher than Hf, whereas is lower than Ti for the (11$\bar{2}$0) surface. Furthermore, down groups VII and VIII the same trend is followed, yet in opposite direction, *i.e.* those with lower number of interacting

atoms have larger E_{ads}. These exceptions can be interpreted as that there is a clear trend comparing atoms from a period but not down the same group.

7.3.2. d-Band Centre

As before said, there appears to be a correlation between the number of *d* electrons and the CO stability. This made us think that the *d*-band model, as firstly postulated by Hammer and Nørskov, could be applied.[14] There, the authors stated that the chemical activity of a TM surface could be seized by the *d*-band centre, which is nothing else but the gravimetric centre of the density of states of the *d*-band, including empty and occupied states, while considering the last occupied level, *i.e.* the Fermi level, as a reference. Thus, a negative *d* band center, ε_d, implies that the majority of states are occupied, and so, stable, and therefore, less active, while positive ε_d, implies that the majority of states are unoccupied and at high energies, thus eager to stabilize by bonding, and so implying a higher chemical activity. Here we evaluated the applicability of the *d*-band centres, taken from a previous study carried out at the same computational level.[18] The results show a very good linear trend, in the expected direction, mostly kept even when distinguishing in between surfaces, and so, the *d*-band centre, mostly applied on *fcc* TMs, seems to be valid across the *d*-series, as proven right on *hcp* metals.

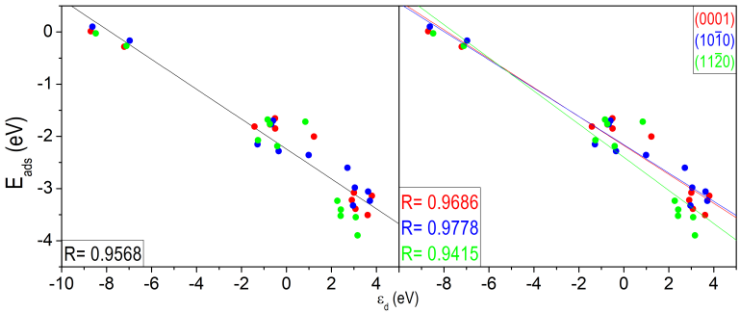

Figure 21: Trends of the E_{ads} *vs.* the *d*-band centre, ε_d, altogether (left), or decomposed by the different surfaces (right).

7.3.3. *Surface energy*

Another descriptor that has been alleged to affect the adsorption energy is the surface energy; the idea behind is rather simple; a very stable surface, with a small surface energy, γ, would be less eager to adsorb something upon to compensate its instability. The other way around, when it features a high surface energy, implies that is more unstable, and so more

active. To certify this, a representation of the E_{ads} with respect the surface energy, γ, has been done, whose values were obtained in a previous work at the same computational level, see Figure 22,[19] and showing a certain trend that, the smaller the surface energy, the weaker the E_{ads}, although the linearity achieved is clearly poor, specially compared to the *d*-band centre, so that γ should be treated more as a qualitative descriptor.

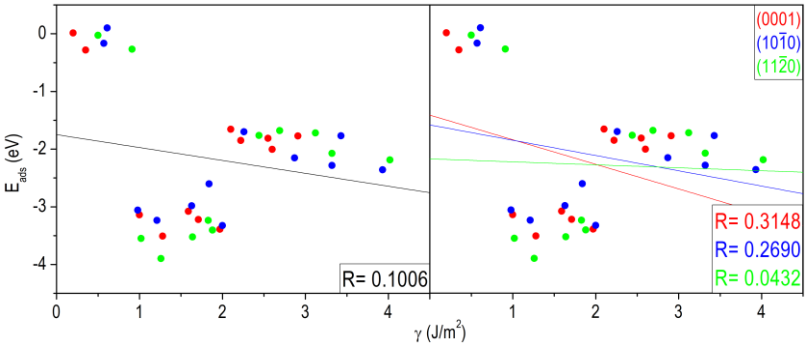

Figure 22: E_{ads} *vs.* surface energy trends, altogether (left) or decomposed by the different surfaces (right).

7.3.4. *Height*

Another tested trend has been the height of the CO respect of the surface. For consistency, this distance is measured as the difference of the average height of all surface metal atoms to the mean height of the CO molecule, *h*, equivalent to the height of the centre of the CO bond length. Thus, the height of the most stable position increases along the periods, see Figure 23.

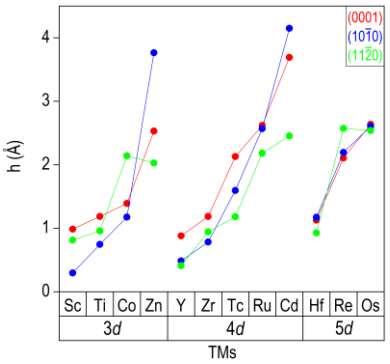

Figure 23: Representation of the height, *h*, of each CO molecule on the most stable position on each TM surface

This can be easily interpreted as a relation between *h* and E_{ads}. When the interaction is stronger, the molecule gets closer. This backs up the previous trend referred to the number interacting TM atoms, because when the molecule is closer to the surface, it may start interacting with the subsurface metal atoms. However, when looking into the groups, such relation is not evident. As above commented, when going down a group the number of TM atoms that interact with the CO decreases and, consequently, the height should increase, yet there are many exceptions to this. Some groups feature a height increase or decrease depending on the analysed surface. Consequently, it appears that such a trend is nothing but a reflection of the previously observed one on E_{ads}.

7.3.5. *C-M bond length*

Another physical value that can show a trend with the E_{ads} is the length of the bond between the C and the metal atoms of the surface, the *d*(CM). Thus, the *d*(CM) would get shorter alongside the adsorption strength gets greater. This is visible in Figure 24. However, even though the trend is captured, the correlation is rather poor, and the trend probably biased by the farther and weaker points; therefore this statement should be taken with caution.

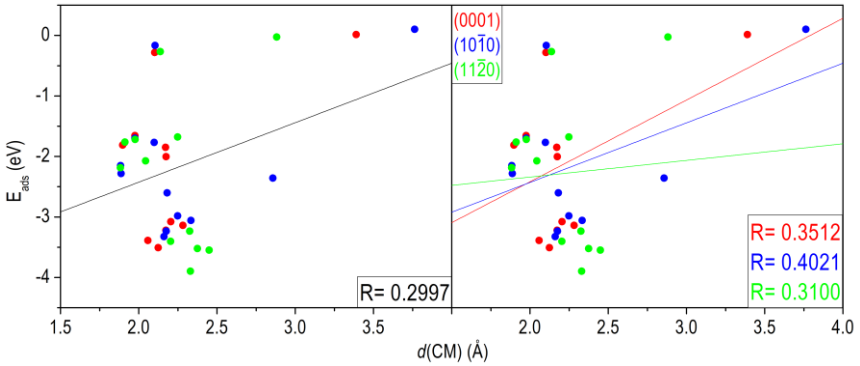

Figure 24: Representation of the relation between the length of the C-Metal bond and the E_{ads}.

7.4. CO BOND

As aforementioned, the adsorption process affects the strength of the CO bond through the donation/back-donation mechanism. The donation is responsible of the σ-bonding with the surface, whereas the back-donation fills with electron density a $2\pi^*$ anti-bonding CO orbital, effectively reducing its bond order, and so, making the bond weaker and longer. The results of it can be seized thus examining the CO bond length, and also can be detected by the molecular IR spectrum. Note by passing by that the CO bond is maintained, and so, there is no spontaneous dissociation upon adsorption.

7.4.1. *CO bond length*

The elongation of the C-O bond, *d*(CO), can be observed as well when analysing the same position on different surfaces. The most common, representative case, is when the CO is adsorbed on a Top position in a perpendicular fashion (η^1-CO-μ^1-C_T), *e.g.* on the $(10\bar{1}0)$ surface. As one can see in Figure 25, those TMs that feature this exact position have longer *d*(CO) values, as such an arrangement maximizes the donation/back-donation mechanism.

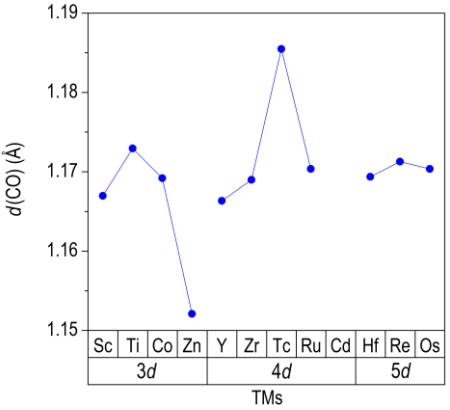

Figure 25: Representation of the *d*(CO) bond length for the CO molecule adsorbed on a η^1-CO-μ^1-C_T position on the example case of TM $(10\bar{1}0)$ surfaces.

Aside from that, when comparing the bond lengths of most stable positions there is as well a relation. Those TMs from Groups III and IV tend to have a higher number of interacting atoms, and so have longer distances than the ones from the groups VII to IX and XII, see Figure 26. This can be interpreted as the effect of the formation of bonds between C and O atoms with the surface at the expense of the integrity of the CO molecule.

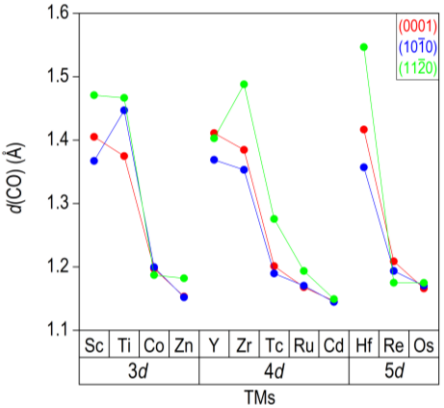

Figure 26: Representation of the *d*(CO) bond length of CO molecule adsorbed on most stable positions on each studied TM surface.

7.4.2. *IR Spectra*

The vibrational frequencies of the adsorbed CO were simulated for all most stable positions of CO on each of the studied TM surfaces, following a procedure well established in the past, where frequencies are obtained by Hessian construction by finite differences of 0.03 Å, and diagonalized.[38,39] The main result that can be seen is a decrease of the CO stretching vibrational frequency, as a direct result of the CO bond weakening, plus, due to the dipole selection rule, that the intensities change, being the more perpendicular situations the more intense. All the (0001), (10$\bar{1}$0), and (11$\bar{2}$0) surfaces simulated IR spectra are encompassed in Appendix 2.

Going into a more fine detail, when a bond becomes weaker than originally is, its stretching frequency decreases. Thus, when the CO molecule interacts through both the C and O atoms it features smaller characteristic CO stretching vibrational frequency, ν(CO), see Figure 27. Such intensity changes are biased by the final position of the CO being parallel or perpendicular, see for instance in Figure 28 the excellent regression of the natural logarithm of the ν(CO) intensity change with respect the sinus of the angle of the CO bond with respect the surface plane. Notice that this angular change of the molecule with respect the surface still provokes that some of the frustrated translation and rotation movements, with a non-zero component of the dipole moment perpendicular to the surface, become now visible to IR spectrum, invisible otherwise, and appreciated in some of the spectra shown in Appendix 2.

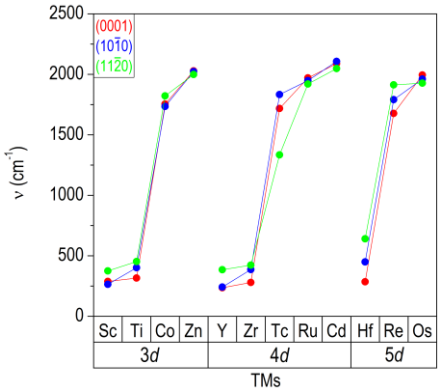

Figure 27: Representation of the CO stretching frequency, ν(CO), for the most stable CO adsorption site on each studied TM.

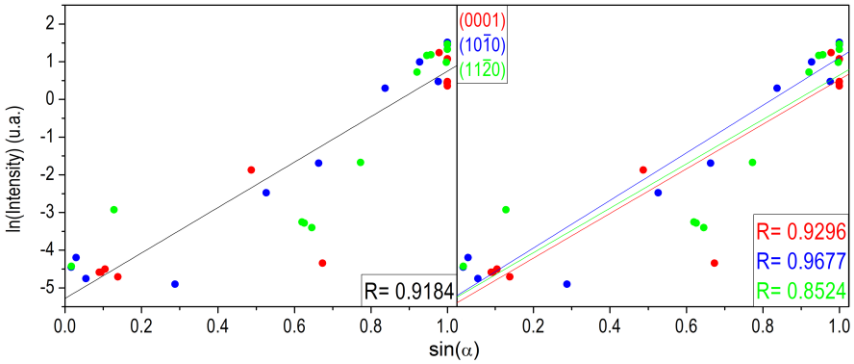

Figure 28: Trends of the natural logarithm of the maximum intensity of the IR spectra with respect the sinus of the CO bond angle with respect the surface.

7.4.3. *Dissociation*

Finally, earlier it has been shown that the CO bond normally gets weaker. One could think that, the weaker the bond, the easier would be the CO dissociation, and, actually, the CO bond scission is critical in diverse chemically appealing processes, as the Fischer-Tropsch catalysis, converting CO into hydrocarbons, and normally catalysed by late TMs.[40] Here this second process, this is, the CO breaking after its adsorption, is assessed, as those early TMs feature longer *d*(CO) values, and parallel conformations, which could be indicative that those are able to catalyse such a process. To analyze this, we computed the dissociation energy of the CO molecule on the studied surfaces. For so, we use the adsorption energies of C and O atoms, as earlier obtained using the same computational setup.[30,31] Thus, the dissociation energy with

respect the CO molecule in vacuum can be easily treated as its dissociation in vacuum, followed by the adsorption of the atomic C and O fragments. This dissociated energies are shown in Table 2; but, more importantly, is the difference in energy in between E_{ads} and E_{dis}, here named ΔE. When such a ΔE is negative, it would imply that the CO fragmentation on the surface would be thermodynamically favourable, although one has to keep in mind that no kinetic energy barriers are being here calculated, which, being high, could prevent such a process to happen. Otherwise, when the ΔE is very positive, implies that the CO dissociation is endothermic, and that the energy barriers would be, at least, that ΔE high. A careful analysis of the values clearly illustrates the preference of early TMs for CO dissociation, while this gets reduced when going along the *d* series, being the late TMs the least likely to dissociate the CO bonds.

TM	(0001)		$(10\bar{1}0)$		$(11\bar{2}0)$	
	E_{dis}	ΔE	E_{dis}	ΔE	E_{dis}	ΔE
Sc	-6.44	-2.93	-2.38	0.85	-5.98	-2.28
Y	-5.92	-2.78	-4.55	-1.49	-5.43	-1.88
Ti	-6.09	-2.70	-3.14	0.19	-5.44	-2.04
Zr	-6.20	-3.12	-4.50	-1.52	-4.13	-0.61
Hf	-6.51	-3.29	-5.07	-2.47	-6.19	-2.95
Tc	-1.66	0.19	-2.39	-0.63	-1.36	0.31
Re	-2.37	-0.37	-2.34	0.02	-1.57	0.15
Ru	-1.39	0.42	-1.18	0.97	-1.69	0.39
Os	-1.26	0.51	-1.02	1.27	-1.88	0.31
Co	-0.51	1.15	-0.42	1.28	-0.95	0.81
Zn	4.23	4.51	4.59	4.75	6.38	6.64
Cd	3.32	3.30	3.90	3.79	2.77	2.79

Table 2: E_{dis} and ΔE values, both in eV, for each TM and surface.

8. CONCLUSIONS

The following itemized conclusions can be withdrawn after the analysis of the obtained data:

- The CO is found to be adsorbed either through the C atom or through both molecular atoms, or not adsorbed at all, as found on late TMs, but never solely attached by its O atom.
- While increasing the number of *d* valance electrons of the TM, the CO tends to pass from an interaction with both atoms, to just through the C, to, eventually, no interaction.
- New adsorption positions have been found for the CO molecule when attached to some of the investigated $(10\bar{1}0)$ and $(11\bar{2}0)$ TM surfaces, few resulting from some surface reversible reconstruction, although some other non-reversible reconstructions were observed and used as references.
- A main factor that outlines the E_{ads} strength seems to be the number of atoms from the surface involved in the CO attachment.
- The *d*-band centre is found to be a rather good quantitative descriptor of the CO adsorption strength, applicable to the full length of the *d* TM series.
- A qualitative trend is found in between surface energies and E_{ads}.
- A donation/back-donation type mechanism is found for the CO perpendicular adsorption, which enlarges the CO bond length.
- The IR spectra show a decrease of the stretching frequency as a result of the CO bond weakening, and so, related to the number of TM atoms involved in the interaction or the *d*-band position.
- Those CO molecules that are adsorbed parallel to the surface have a decreased ν(CO) stretching vibration intensity due to the surface dipole selection rule, yet other frustrated rotations and translations may have some significant IR component.
- A thermodynamic analysis reveals that CO dissociation seems to be more feasible on early TMs, and more difficult on late TMs.

9. REFERENCES

1. Pischel, J.; Pucci, A. Low-temperature adsorption of carbon monoxide on gold surfaces: IR spectroscopy uncovers different adsorption states on pristine and rough (111). *J. Phys. Chem. C* **2015**, *119*, 18340-18351.
2. Weststrate, C.J.; Lundgren, E.; Andersen, J.N.; Rienks, E.D.L.; Gluhoi, A.C.; Bakker, J.W.; Groot, I.M.N.; Nieuwenhuys, B.E. CO adsorption on Au(310) and Au(321): 6-Fold coordinated gold atoms. *Surf. Sci.* **2009,** *603*, 2152-2157.
3. Yang, H. J.; Minato, T.; Kawai, M.; Kim, Y. STM Investigation of CO Ordering on Pt(111): From an isolated molecule to High-Coverage Superstructures, *J. Phys. Chem. C* **2013**, *117*, 16429-16437.
4. Gajdoš, M.; Eichler, A.; Hafner, J. CO adsorption on closed-packed transition and noble metal surfaces: trends from *ab initio* calculations. *J. Phys.: Condens. Matter* **2004**, *16*, 1141.
5. Peterson, A. A.; Grabow, L.C.; Brennan, T.P.; Shong, B; Ooi, C.; Wu, D.M.; Li, C.W.; Kuchwaha, A.; Medford, A.J.; Mbuga, F.; Li, L.; Nørskov, J.K. Finite-size effects in O and CO adsorption for the late transition metals. *Top. Catal.* **2012**, *55*, 1276-1828.
6. Borji, F.; Pur, A.N.; Karimi, J.; Izadyar, M. The molecular adsorption of carbon monoxide on cobalt surfaces: a DFT study. *Prog. React. Kinet. Mec.* **2017**, *42*, 89-98.
7. Jiang, L.; Xu, Q. Theorietical study of the interaction of carbon monoxide with 3d metal dimmers. *J. Chem. Phys.* **2008**, *128*, 124317.
8. Jiang, L.; Xu, Q. Density functional theory study of the interaction of carbon monoxide with the second-row transition-metal dimmers. *Chem. Phys.* **2008**, *354*, 32-37.
9. Wu, G.; Wang, J.; Lu, Y.; Yang, M. Density functional study of CO adsorption on Sc_n (n=2-13) clusters. *J. Chem. Phys.* **2008**, *128*, 224315.
10. Xu, Q.; Jiang, L.; Tsumori, N. *cyclo*-$Ti_3[\eta^2(\mu_2\text{-}C,O)]_3$: A side-on-bonded polycarbonyl titanium cluster with potentially anitaromatic character. *Angew. Chem. In. Ed.* **2005***, 44*, 4338-4342.
11. Bengum, P.; Deka, R. C. A comparative DFT study on the catalytic oxidation of nitric oxide by Pd_2 and PdM (M=Cu, Rh, Ag, Au, Pt). *Catal. Lett.* **2017,** *147*, 581-591.
12. Krajčí, M.; Hafner J. Intermatellic compound AlPd as a selective hydrogenation catalyst: A DFT study. *J. Phys. Chem.* **2012**, *116*, 6307-6319.
13. Andersson, M. P.; Bligaard, T.; Kustoc, A.; Larsen, K.E.; Greeley, J.; Johannessen, T.; Christensen, C.H.; Nørskov, J.K. Toward computational screening in heterogeneous catalysis: Pareto-optimal methanation catalysts. *J. Catal.* **2006**, *239*, 501-506.
14. Hammer, B.; Nørskov, J.K. Electronic factors determining the reactivity of the metal surfaces. *Surf. Sci.* **1995**, *343*, 211-220.
15. Zhuang, H.; Tkalych, A.J.; Carter, E.A. Surface Energy as a Descriptor of Catalytic Activity. *J. Phys. Chem. C* **2016**, *120*, 23698-23706.
16. Hohenberg, P.; Kohn, W. Inhomogeneous electron gas. *Phys. Rev. B* **1964**, *136***,** 864.
17. Khon, W.; Sham, J. Self-consistent equations including exchange and correlation effects. *Phys. Rev. A* **1965***, 140*, 1133.
18. Janthon, P; Kozlov, S. M.; Viñes, F.; Limtrakul, J.; Illas, F. Establishing the accuracy of broadly used density functionals in describing bulk properties of transition metals. *J. Chem. Theory. Comput.* **2013**, *9*, 1631-1640.

19. Vega, L.; Ruvireta, J; Viñes, F; Illas, F. Jacob's ladder as skeched by escher: Assessing the performance of broadly used density functionals on transition metals surface properties. *J. Chem. Theory Comput.* **2018**, *14*, 395-403.
20. Vega, L.; Martínez, B.; Viñes, F.; Illas, F. Robustness of surface activity electronic structure-based descriptors of transition metals. *Phys. Chem. Chem. Phys.* **2018**, *20*, 20548-20554.
21. Kittel, C. *Introduction to solid state physics,* 8th ed.; Wiley: United States of America, **2005**.
22. Wang, S.; Cao, D.; Li, D.; Wang, J; Jiao, H. Chemisorption of CO_2 on nickel surfaces. *J. Phys. Chem. B* **2005**, *109*, 18956-18963.
23. Lavrich, D. J.; Wetterer, S. M.; Bernasek, S. L.; Scoles, G. Physisorption and chemisorption of alkanethoils and alkyl sulfides on Au(111). *J. Phys. Chem. B* **1998**, *102*, 3456-3456.
24. Doyen, G. Theory of carbon monoxide chemisorptions on transition metals. *Surf. Sci.* **1974**, *43*, 197-229.
25. Dimakis, N.; Navarro, N.; Mion, T.; Smotkin, E. S. Carbon monoxide adsorption coverage study on Platinum and Ruthenium Surfaces. *J. Phys. Chem. C* **2014**, *118*, 11711-11722.
26. Valcárcel, A.; Ricart, J.M.; Illas, F.; Clotet, A. Theoretical Interpretation of the IR Spectrum of Propyne on Cu(111). *J. Phys. Chem. B.* **2004**, *208*, 18297-18305.
27. Kresse, G.; Furthmüller, J. Efficient iterative schemes for *ab initio* total-energy calculation using plain-wave basis set. *Phys. Rev. B* **1996,** *54*, 11169.
28. Perdew, J. P.; Burke, K.; Ernzerhof, M. Generalized gradient approximation made simple. *Phys. Rev. Lett.* **1996,** *77*, 3865.
29. Janthon, P.; Viñes, F.; Sirijaraensre, J.; Limtrakul, J.; Illas, F. Adding Pieces to the CO/Pt (111) Puzzle: The Role of Dispersion. *J. Phys. Chem. C* **2017**, *121*, 3970-3977.
30. Jurado, A. TFM. First-principles evaluation of the initial oxidation of transition metal surfaces, Universitat de Barcelona, 2019.
31. Piqué, O. TFM. Interplay of Carbon on Transition Metal Surfaces and Nanoparticles, Universitat de Batcelona, 2018.
32. Monkhorst, H. J.; Pack, J. D. Special points for Brillouin-zone integrations. *Phys. Rev. B* **1976,** *13*, 5188.
33. The PAW and UP-PP database. https://www.vasp.at/vasp-workshop/pseudoppdatabase.pdf (accessed Feb 21, 2020).
34. Abild-Pedersen, F.; Andersson, M.P. CO adsorption energies on metals with correction for high coordination adsorption sites – A density functional study. *Surf. Sci.* **2007**, *601*, 1747-1753
35. Hammer, B.; Hansen, L. B.; Nørskov, J. K. Improved adsorption energetic within density-functional theory using revised Perdew-Burke-Ernzerhof functionals. *Phys. Rev. B* **1999**, *59*, 7413-7421.
36. Burke, K.; Perdew, J. P.; Wang, Y. Correlation hole of the spin-polarized electron gas, with exact small-wave-vector and high-density scaling. *Phys. Rev. B.* **1991**, *44*, 13298.
38. Luckas, N.; Viñes, F.; Happel, M.; Desikusumastuti, A.; Libuda, J.; Görling, A. Density Funtional Calculations and IR Reflection Absorption Spectroscopy on the Interaction of SO_2 with Oxide-Supported Pd Nanoparticles. J. Phys. Chem. C **2010**, *114*, 13813-13824.
39. Happel, M.; Luckas, N.; Viñes, F.; Sobota, M.; Laurin, M.; Görling, A.; Libuda, J. SO_2 Adsorption on Pt(111) and Oxygen Precovered Pt(111): A Combined Infrared Reflection Absorption Spectroscpoy and Density Functional Study. J. Phys. Chem. C **2011**, *115*, 479-491.
40. Cheng, J.; Hu, P.; Ellis, P.; French, S.; Kelly, G.; Lok, C.M. Some Understanding of Ficher-Tropsch Synthesis from Density Functional Theory Calculations. *Top. Catal.* **2010**, *53*, 326-337

10. ACRONYMS

bcc: body-centered cubic

BO: Born-Oppenheimer

DFT: Density Functional Theory

fcc: face-centered cubic

GGA: Generalized Gradient Approximation

hcp: hexagonal closed-packed

HF: Hartree-Fock

HOMO: Highest Occupied Molecular Orbital

IR: Infrared

LDA: Local Density Approximation

PAW: Projector Augmented Wave

PBC: Periodic Boundary Conditions

PBE: Perdew-Burke-Ernzerhof

STM: Scanning Tunnelling Microscopy

TM: Transition Metal

VASP: Vienna *Ab initio* Simulation Package

xc: exchange-correlation

XPS: X-ray Photoemission Spectroscopy

XRD: X-Ray Diffraction

APPENDICES

APPENDIX 1: POSITIONS TAGS FOR ALL SURFACES

Table 1a: Final stable position tags on the (0001), (10$\bar{1}$0), and (11$\bar{2}$0) surfaces of the explored TMs, alongside with the cases where such a mínima is located, including the metals where such are found to be the most stable site, shown in bold.

(0001) Position	TM
η^1-CO-μ^1-C_T	Y, Ti, Zr, Hf, Tc, Re, Co, Zn, **Ru, Os**
η^1-CO-μ^2-C_B	Os, Co
η^1-CO-μ^4-C_H	Ti, Zr, Hf, Tc, Re ,Ru, Os, **Co**
η^1-CO-μ^3-C_{H_E}	Ru, Co, **Tc, Re**
η^2-CO-μ^4-C_HO_T	Sc, Y
η^2-CO-μ^4-C_HO_B	Sc
η^2-CO-μ^5-$C_HO_{H_E}$	**Sc, Y, Ti, Zr, Hf**
η^2-CO-μ^3-$C_{H_E}O_T$	Sc, Y, Ti, Zr, Hf
η^2-CO-μ^5-$C_{H_E}O_H$	Sc, Y, Ti, Zr, Hf
—[a]	**Zn, Cd**

[a] No quantifiable interaction; physisorption state.

(10$\bar{1}$0) Position	TM
η^1-CO-μ^1-C_T	Sc, Y, Ti, Zr, Hf, Co, Re, **Ru, Os, Zn**
η^1-CO-μ^2-C_{B_S}	Sc, Y, Ti, Zr, Hf, Tc, Ru, Os, Co, Zn, **Tc, Re**
η^1-CO-μ^4-C_{B_L}	Y, Ti, Zr, Hf, Tc, Re, Ru, Os, Co, Zn
η^1-CO-μ^1-C_H	Y, Ti, Zr, Hf, Tc, Re, Ru, Os, Co, Zn
η^1-CO-μ^3-$C_{H_{2T}}$	Tc, **Co**
η^2-CO-μ^2-$C_{B_S}CO_T$	Sc, Y, Ti, Zr, Hf
η^2-CO-μ^4-$C_{BL_L}O_T$	Ti, Zr, Hf

η^2-CO-μ^4-$C_{BL_L}O_{B_S}$	Sc
η^2-CO-μ^4-$C_{BL_L}O_H$	Y, Ti, Zr, Hf
η^2-CO-μ^5-$C_{BL_L}O_{H_{2T}}$	Sc, **Ti**
η^2-CO-μ^3-$C_{H_{2T}}O_{B_S}$	Sc, Y, Ti, Zr, **Hf**
η^2-CO-μ^3-$C_{H_{2T}}O_H$	Y, Hf, Zr
η^2-CO-μ^5-$C_{H_{2T}}O_{H_{2T}}$	Ti
η^2-CO-μ^4-$C_{H_{2T}}O_{H_{2B}}$	Sc, Y, Hf
η^2-CO-μ^4-$C_{H_{2B}}O_{H_{2T}}$	Sc
η^2-CO-μ^4-$C_{H_{2B}}O_{H_{2B}}$	**Sc, Y, Zr**
—[a]	Zn, **Cd**

[a] No quantifiable interaction; physisorption state.

(11$\bar{2}$0) Positions	**TM**
η^1-CO-μ^1-C_T	Ti, Zr, Hf, Tc, Ru, Co, **Re, Os**
η^1-CO-μ^2-C_{B_S}	Sc, Y, Ti, Zr, Hf, Tc, Os, Zn, **Ru, Co, Zn**
η^1-CO-μ^2-C_{B_L}	Ru, Os, Zn, **Cd**
η^1-CO-μ^4-C_{BL_L}	Tc, Re, Co
η^1-CO-μ^2-$C_{B_{SD}}$	Sc, Y, Ti, Zr, Hf
η^1-CO-μ^4-$C_{B_{LD}}$	Ru, Co
η^1-CO-μ^1-C_H	Hf
η^2-CO-μ^2-C_TO_T	Ru, Os
η^2-CO-μ^4-$C_{B_L}O_T$	Ti, **Tc**
η^2-CO-μ^5-$C_{BL_L}O_T$	Zr, Hf
η^2-CO-μ^4-$C_{BL_L}O_H$	Y
η^2-CO-μ^5-$C_{BL_L}O_{H_{2T}}$	Sc
η^2-CO-μ^3-$C_{B_{SD}}O_T$	Hf
η^2-CO-μ^4-$C_{B_{LD}}O_T$	Hf

η^2-CO-μ^4-$C_{B_{LD}}O_{B_S}$	Sc, Y
η^2-CO-μ^5-$C_{B_{LD}}O_{B_{SD}}$	Sc, **Y**
η^2-CO-μ^5-$C_{B_{LD}}O_{B_{LD}}$	Y
η^2-CO-μ^4-C_HO_T	Sc, Y, Ti
η^2-CO-μ^5-$C_HO_{B_S}$	Ti, Zr, **Sc**
η^2-CO-μ^5-$C_HO_{B_{SD}}$	Sc, Y, **Ti, Zr, Hf**
η^2-CO-μ^4-$C_{H_{2T}}O_{H_{2T}}$	Sc
—[a]	Zn

[a] No quantifiable interaction; physisorption state.

APPENDIX 2: IR SPECTRA

Figure 2a: Simulated IR spectra of CO adsorbed on its most stable position on the (0001), (10$\bar{1}$0), and (11$\bar{2}$0) surfaces of the explored TMs, alongside with the isolated CO molecule vibration.

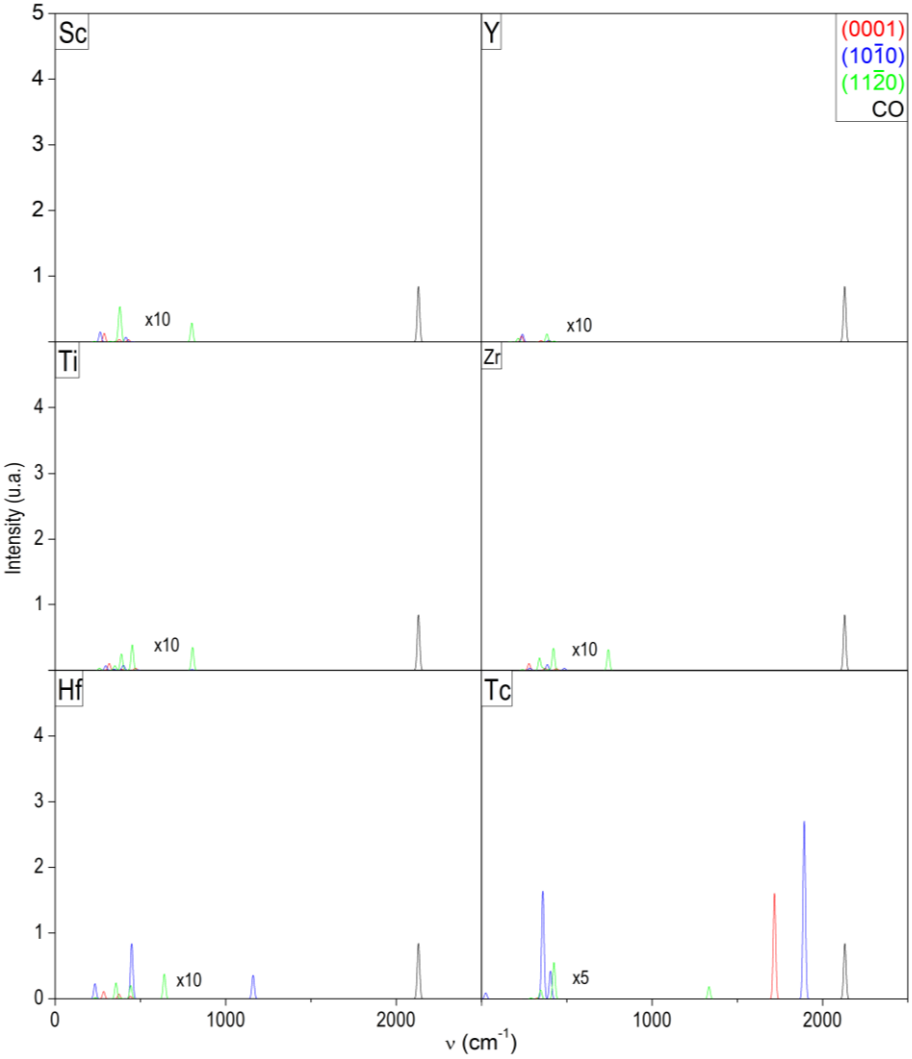

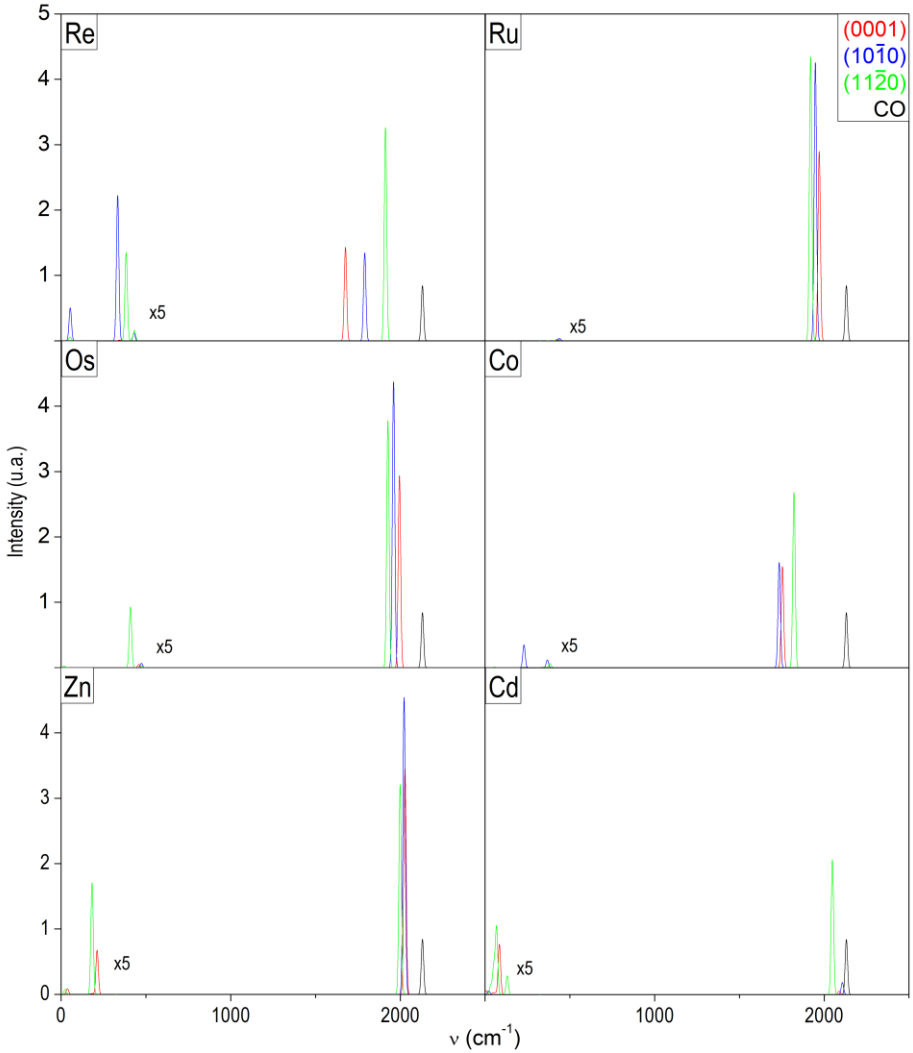
Re
Ru
Os
Co
Zn
Cd
(0001)
(10$\bar{1}$0)
(11$\bar{2}$0)
CO
x5
Intensity (u.a.)
ν (cm^{-1})
0
1000
2000
1
2
3
4
5